Nonwetting of impinging droplets on textured surfaces

Tao Deng, Kripa K. Varanasi, Ming Hsu, Nitin Bhate, Chris Keimel, Judith Stein, and Margaret Blohm

Citation: Appl. Phys. Lett. **94**, 133109 (2009); doi: 10.1063/1.3110054
View online: http://dx.doi.org/10.1063/1.3110054
View Table of Contents: http://aip.scitation.org/toc/apl/94/13
Published by the American Institute of Physics

Nonwetting of impinging droplets on textured surfaces

Tao Deng,[1,a),b)] Kripa K. Varanasi,[2,a),c)] Ming Hsu,[1] Nitin Bhate,[1] Chris Keimel,[1] Judith Stein,[1] and Margaret Blohm[1]
[1]*Nanotechnology Advanced Technology, GE Global Research Center, One Research Circle, Niskayuna, New York 12309, USA*
[2]*Department of Mechanical Engineering, Massachusetts Institute of Technology, Cambridge, Massachusetts 02139, USA*

(Received 22 February 2009; accepted 10 March 2009; published online 2 April 2009)

This paper studies the impinging droplets on superhydrophobic textured surfaces and proposes a design guideline for nonwetting surfaces under droplet impingement. A new wetting pressure, the effective water hammer pressure, is introduced in the study to clearly define wetting states for the impinging droplets. This approach establishes the design criteria for nonwetting surfaces to impinging droplets. For impingement speed higher than raindrop speed, the surfaces need to have sub-100-nm features to generate a large enough antiwetting pressure for the droplets to take a nonwetting state after impingement. © *2009 American Institute of Physics*.
[DOI: 10.1063/1.3110054]

The study of droplet impingement process has been an active research area in both experimental investigation and theoretical modeling for more than a century.[1–7] The understanding of the physics of droplet impingement will greatly help design surfaces that minimize droplet erosion, reduce the moisture-induced efficiency losses in steam turbines, and minimize the ice formation on aircraft and wind turbine external surfaces. During the past several years, some research groups started exploring water droplet impingement on textured superhydrophobic surfaces.[6,8–11] Superhydrophobic surfaces are surfaces that mimic the Lotus leaf,[12] and various research groups studied the wetting states of stationary droplets on superhydrophobic surfaces.[13–15] Many applications, however, involve impinging droplets rather than stationary droplets. The study of wetting states on superhydrophobic surfaces for impinging droplets thus is important to these applications. When droplets impinge on a textured surface, the states of wetting depend on the balance of wetting pressure (P_{wetting}) and antiwetting pressure ($P_{\mathrm{antiwetting}}$).[8–10] A larger P_{wetting} over $P_{\mathrm{antiwetting}}$ causes droplets to wet the surface. Most of previous studies of the wetting states for impinging droplets with density ρ and velocity V used dynamic pressure [P_D, Eq. (1)] as the sole wetting pressure and resulted in only two wetting states (bouncing and sticky),

$$P_D = \tfrac{1}{2}\rho V^2. \tag{1}$$

The use of single wetting pressure P_D cannot explain the partial wetting state observed in the experiments and leads to insufficient design of nonwetting surfaces for impinging droplets.

This paper introduces a new wetting pressure and uses two wetting pressures, an effective water hammer pressure (P_{EWH}) at the contact stage and P_D at the spreading stage of the impingement, to define three wetting states for the impinging droplet: wetting, partial wetting, and nonwetting. A two-stage (contact stage and spreading stage) approach has been used in the studies of droplet impingement on flat surfaces.[3,16–18] In the contact stage, the initial impact of the droplet onto the flat surfaces generates a water hammer pressure (P_{WH}) due to the compression of liquid behind the shock wave envelope.[3,16–18] At the spreading stage, the shock wave overtakes the outward moving contact line. The pressure is released, and at this stage the pressure drops to P_D. For a textured surface, P_{WH} will also be generated at the contact stage when water is compressed behind the shock wave envelope. When the shock front moves to the edge of the textures, for example, the edge of a single post, the compressed liquid suddenly has free space to expand. The water-air interface thus experiences a push from the compressed region with a pressure that is on the order of P_{WH}. We refer to this pressure as P_{EWH} in this study. For the purpose of exploring the design guideline for surfaces that resist maximum wetting pressure, we will use the value of P_{WH} as the upper bound estimation of P_{EWH} in our discussion because P_{WH} is the maximum possible wetting pressure experienced by the water-air interface. For textured surface, $P_{\mathrm{antiwetting}}$ is the capillary pressure (P_C) generated within the surface textures.[8–10] With two wetting pressures and one antiwetting pressure, there will be three wetting states (Fig. 1).

As schematically shown in Fig. 1, when structures are sparse, P_C is small and droplets tend to be pinned after the

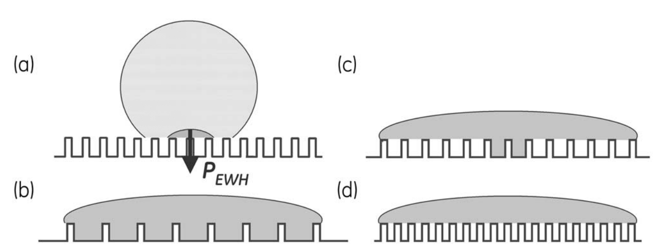

FIG. 1. Relative magnitude of the wetting and antiwetting pressures decides the wetting states of impinging droplets: (a) P_{EWH} is generated during the contact stage as the droplet impinges on the textured surface. (b) Total wetting state ($P_{\mathrm{EWH}} > P_D > P_C$) as water penetrates in both contact and spreading stage. (c) Partial wetting state ($P_{\mathrm{EWH}} > P_C > P_D$) as water penetrates only during contact stage. (d) Total nonwetting state ($P_C > P_{\mathrm{EWH}} > P_D$) as the structure resist wetting in both stages.

[a)]Authors to whom correspondence should addressed. Electronic addresses: dengt@research.ge.com and varanasi@mit.edu.
[b)]Tel.: 518-387-5473. FAX 518-387-7548.
[c)]Tel.: 617-324-5608. FAX 617-253-7549.

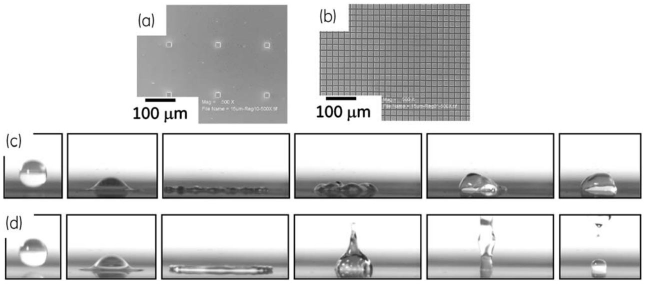

FIG. 2. (a) Top view SEM of the silicon post array with $A \sim 15$ μm, $B \sim 150$ μm, and $H \sim 20$ μm. (b) Top view SEM of the silicon post array with $A \sim 15$ μm, $B \sim 5$ μm, and $H \sim 20$ μm. (c) Sequential video images of droplet impinging on the surface of (a). The water droplet eventually stayed pinned to the surface due to the large wetted interface. (d) Sequential video images of droplet impinging on the surface of (b). The water droplet eventually pinched off, with small portion of the droplet staying on the surface due to the small wetted interface.

impingement [Figs. 1(b) and 1(c)]. In the experiment, water droplets were indeed pinned on two sparsely patterned silicon post arrays (Fig. 2). The silicon posts were fabricated using standard photolithography process and modified with a thin coating of (tridecafluoro-1,1,2,2-tetrahydrooctyl) trichlorosilane (Gelest, Inc., Morrisville, PA) through vapor phase deposition. The water droplets used in the experiment had diameters of ~ 1 mm and velocity of ~ 3 m/s. A high-speed camera (up to 40 K frames^{-1}) was used in the study. Due to the shape of the droplet (spherical) and the low impinging speed, the P_{EWH} experienced by the contact region is[3]

$$P_{\mathrm{EWH}} \approx 0.2\rho CV. \tag{2}$$

In Eq. (2), C is the sound velocity in water. The P_{EWH} and P_D of the droplets with impinging speed of 3 m/s are thus calculated to be ~ 0.9 MPa [Eq. (2), $C \sim 1497$ m/s (Ref. 19) and $\rho \sim 1000$ kg/m^3] and ~ 4.5 kPa [Eq. (1)], respectively.

The silicon posts are arranged in a square array with the post width of A, spacing of B, and height of H. With a square array, maximum possible deformation of water-air interface happens between the diagonal posts within the single cell of the array. The contact angle at the water-solid-air interface increases to advancing contact angle when water-air interface reaches maximum possible deformation.[8] The maximum P_C for the square array thus can be calculated as the Laplace pressure of the maximum deformation of the water-air interface between the textures,

$$P_C = -2\sqrt{2}\gamma_{LV} \cos \theta_A / B. \tag{3}$$

In Eq. (3), γ_{LV} is the surface energy of the water at water-vapor interface (~ 0.073 N/m) and θ_A is the advancing contact angle of the water droplet on the flat surface. Different surface intrinsic wettability will change θ_A and P_C, and result in different pressure balance and wetting states. For a flat fluorinated silicon surface, the measured θ_A is $\sim 128°$.

Figure 2(a) shows the top view scanning electron microscope (SEM) image of the silicon posts with $A \sim 15$ μm, $B \sim 150$ μm, and $H \sim 20$ μm. Figure 2(c) shows the sequential images of a water droplet impinging on such surface. The calculated P_C was ~ 0.8 kPa, which was smaller than both P_{EWH} and P_D. The droplet thus penetrated into the textures during both impingement stages, and took a total

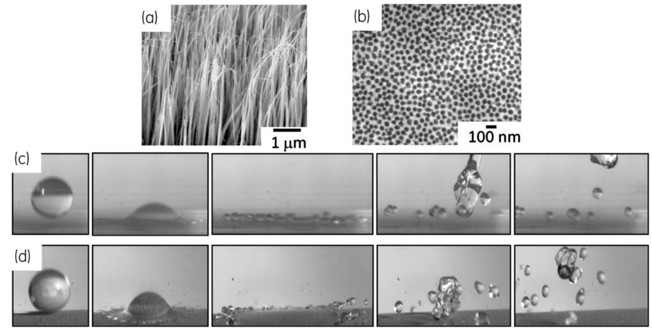

FIG. 3. (a) SEM of silicon nanowires (side view). (b) SEM of AAO surface (top view). (c) Sequential video images of droplet impinging on silicon nanowire surface. The water droplet was eventually completely lifted off the surfaces, with some satellite droplets forming around the main droplet. (d) Sequential video images of droplet impinging on AAO surface. The water droplet was eventually completely lifted off the surfaces, with some satellite droplets forming around the main droplet.

wetting state after the impingement. The second post array [$A \sim 15$ μm, $B \sim 5$ μm, and $H \sim 20$ μm, Fig. 2(b)] was denser than the first array. The P_C increased to ~ 25 kPa, which was smaller than P_{EWH} but larger than P_D. The relation between pressures is the same as in Fig. 1(c) so there was water penetration during the contact stage and no penetration at the spreading stage. The droplet took a partial wetting state after the impingement [Fig. 2(d)].

To minimize water penetration at the contact stage, the textures need to be denser than those in Fig. 2 to have P_C that can balance P_{EWH}. Figure 3(a) shows the SEM image of dense silicon nanowires grown on a silicon wafer. The silicon nanowires were generated when a precleaned silicon wafer was placed in an inductively coupled plasma chamber with a controlled flow of etching gases ($CHF_3/SF_6/Ar$). The silicon nanowires were modified with fluorosilane after the growth. The average width of the wires was ~ 100 nm and spacing ~ 145 nm. Assuming a square array arrangement, the estimated P_C was ~ 0.9 MPa. As discussed previously, since P_{WH} (~ 0.9 MPa) is the upper bound estimation of P_{EWH}, the real P_{EWH} (≤ 0.9 MPa) might be smaller than the P_C generated from the silicon nanowire surface and the droplet would take a nonwetting state. In the experiment the droplet indeed recoiled and completely bounced off the modified silicon nanowire surface, with no penetration of water in both stages [Fig. 3(c)].

Figure 3(b) shows a structure that has a P_C much larger than both P_{EWH} and P_D. The structure is a porous surface of anodized aluminum oxide (AAO) with average pore size of ~ 38 nm and pore-to-pore spacing of ~ 10 nm. This AAO surface was generated in an anodization process [~ 10 min in concentrated sulfuric acid solution (165 g/l) at 5 °C] and a subsequent pore widening process [~ 25 min in 5 wt % phosphoric acid solution at 25 °C]. For such a porous structure, the capillary pressure is calculated based on

$$P_C = -2\gamma_{LV} \cos \theta_A / r. \tag{4}$$

In Eq. (4), r is the diameter of the pores. The θ_A for a flat fluorinated aluminum oxide surface was $\sim 120°$ in the experiment. The calculated P_C was ~ 3.8 MPa, which was much larger than both P_{EWH} and P_D. The images in Fig. 3(d) show that the droplet fully recoiled and completely bounced off the AAO surface, similar to those in Fig. 3(c). There is also an interesting observation of satellite droplets formation in both Figs. 3(c) and 3(d), which might be related to the surface textures and is currently under investigation.

This paper discusses different type of pressures and wetting states experienced by the impinging droplets on textured surfaces. With the introduction of P_{EWH}, three different wetting states are clearly identified. A design guideline is also established to generate surfaces that are completely nonwettable to impinging droplets. Many applications involve droplets with impinging speed larger than raindrop terminal speed (4 m/s for 1 mm raindrop).[20] For example, in aircraft and steam turbine applications, droplets can move tens of or even hundreds of m/s. In such applications, proper design of the surface textures with sub-100-nm structures is essential to avoid possible wetting or partial wetting of the droplets after impingement. The pressure balance discussed here will also help design substrates to control the wetting behavior of the droplets in inkjet or electrohydrodynamic jet printing[21] to achieve high level of lateral resolution.

The Nanotechnology Advanced Technology Program of GE Global Research supported this work. We thank Dr. Gregory O'Neal and Ms. Shannon Okuyama for their support and helpful discussions.

[1]S. S. Cook, Proc. R. Soc. London, Ser. A **119**, 481 (1928).
[2]R. Dhiman and S. Chandra, Phys. Fluids **20**, 092104 (2008).
[3]O. G. Engel, J. Res. Natl. Bur. Stand. **54**, 281 (1955).
[4]M. Qu, Y. Wu, V. Srinivasan, and A. Gouldstone, Appl. Phys. Lett. **90**, 254101 (2007).
[5]K. Shinoda, H. Murakami, S. Kuroda, S. Oki, K. Takehara, and T. G. Etoh, Appl. Phys. Lett. **90**, 194103 (2007).
[6]Z. Wang, C. Lopez, A. Hirsa, and N. Koratkar, Appl. Phys. Lett. **91**, 023105 (2007).
[7]A. M. Worthington, Proc. R. Soc. London **25**, 261 (1876).
[8]D. Bartolo, F. Bouamrirene, E. Verneuil, A. Buguin, P. Silberzan, and S. Moulinet, Europhys. Lett. **74**, 299 (2006).
[9]Y. C. Jung and B. Bhushan, Langmuir **24**, 6262 (2008).
[10]M. Reyssat, A. Pépin, F. Marty, Y. Chen, and D. Quéré, Europhys. Lett. **74**, 306 (2006).
[11]A. Tuteja, W. Choi, J. M. Mabry, G. H. McKinley, and R. E. Cohen, Proc. Natl. Acad. Sci. U.S.A. **105**, 18200 (2008).
[12]W. Barthlott and C. Neinhuis, Planta **202**, 1 (1997).
[13]N. A. Patankar, Langmuir **20**, 7097 (2004).
[14]A. Sidorenko, T. Krupenkin, and J. Aizenberg, J. Mater. Chem. **18**, 3841 (2008).
[15]A. Tuteja, W. Choi, G. H. McKinley, R. E. Cohen, and M. F. Rubner, MRS Bull. **33**, 752 (2008).
[16]F. P. Bowden, and J. E. Field, Proc. R. Soc. London, Ser. A **282**, 331 (1964).
[17]J. E. Field, Wear **233**, 1 (1999).
[18]M. B. Lesser and J. E. Field, Annu. Rev. Fluid Mech. **15**, 97 (1983).
[19]V. A. Del Grosso and C. W. Mader, J. Acoust. Soc. Am. **52**, 1442 (1972).
[20]N. Dingle and Y. Lee, J. Appl. Meteorol. **11**, 877 (1972).
[21]J. Park, M. Hardy, S. J. Kang, K. Barton, K. Adair, D. K. Mukhopadhyay, C. Y. Lee, M. S. Strano, A. G. Alleyne, J. G. Georgiadis, P. M. Ferreira, and J. A. Rogers, Nature Mater. **6**, 782 (2007).